Available online at www.sciencedirect.com
ScienceDirect
Journal of Sound and Vibration 315 (2008) 890–910
JOURNAL OF SOUND AND VIBRATION
www.elsevier.com/locate/jsvi

A method to measure and interpret input impedance of small acoustic components

D. Rodrigues[a,*], C. Guianvarc'h[b], J.-N. Durocher[a], M. Bruneau[b], A.-M. Bruneau[b]

[a]*Laboratoire National de métrologie et d'Essais (LNE), 29 av. Roger Hennequin, 78197 Trappes Cedex, France*
[b]*Laboratoire d'Acoustique de l'Université du Maine UMR CNRS 6613, av. Olivier Messiaen 72085 Le Mans Cedex 9, France*

Received 12 September 2006; received in revised form 7 February 2008; accepted 11 February 2008
Handling Editor: C. Morfey
Available online 1 April 2008

Abstract

Many applications would require to characterize the input behaviour of small acoustic components such as small tubes, small rectangular or circular slits, small cavities (or their associations in the form of one-port passive linear acoustic systems). These applications relate to artificial ears, loudspeakers, microphones miniaturized or not (among other electroacoustic devices), and acoustic tools used in precise measurements. Today, these small components are characterized analytically using modelling wherein viscosity, heat conduction, inertia, and compressibility of the fluid are considered, beyond realistic boundary conditions (no slip conditions and no temperature variations near the walls). But the results are usually obtained with a relative uncertainty greater than 50% (due to the geometrical uncertainties of the components).

Therefore, it is of importance to characterize experimentally the input properties of these kind of components with a good accuracy, that is to say to measure their input impedance with a relative uncertainty of the order of magnitude of 10^{-2}. These measurements were quite impossible until now because the input impedances of such components are usually much greater than those involved in the measuring set-up. Here a measurement procedure is presented which uses the very precise reciprocity calibration method and the corresponding set-up available on the market. The results obtained on classical elements are discussed by comparison between experimental and theoretical results, showing the precision that would be achieved.

1. Introduction

When designing many acoustic devices (artificial ears, loudspeakers, microphones miniaturized or not, among other electroacoustic devices), or when designing other devices using acoustic tools (for example for precise measurements of Boltzmann constant [1]), dimensions of the acoustic parts of these devices can have the same order of magnitude or can be lower, even much lower, than the acoustic wavelengths considered. In these devices (usually described using lumped-elements circuits in the lower frequency range), damping, elasticity, and inertia can be obtained, respectively, by means of small acoustic components, i.e. narrow tubes or slits, small cavities, and short tubes. Because these acoustic components are widely used, their analytical

*Corresponding author. Tel.: +33 130691487; fax: +33 130691234.
E-mail address: dominique.rodrigues@lne.fr (D. Rodrigues).

0022-460X/$ - see front matter © 2008 Elsevier Ltd. All rights reserved.
doi:10.1016/j.jsv.2008.02.017

Nomenclature

a	radius of the cylindrical cavity
a_t, a_r	radius of the transmitting and receiving diaphragms
a_T	radius of the tubes
$a_\mu b_{\mu\nu}$	normalization coefficient of the eigenfunctions $\psi^d_{\mu\nu}$
$\mathscr{A}$	total area of the walls of the cylindrical cavity
c_0	adiabatic speed of sound
C_P, C_V	specific heat coefficient at constant pressure and constant volume, respectively, per unit of mass
e	thickness of the slit
e_1	dimension of the annular cavity: thickness of the first slit
e_2	dimension of the annular cavity: thickness of the second slit
G	the Green function
i_t	current through the transmitting microphone
k_0	adiabatic wavenumber
k_t	complex wavenumber in the tubes
k_v, k_h	wavenumbers associated with the vortical and the entropic movements
k_z	complex wavenumber in the cylindrical cavity
ℓ	length of the cylindrical cavity
ℓ_c	location along the z-axis in the cylindrical cavity of the acoustic component to be characterized
ℓ_T	length of the tubes
ℓ'_v, ℓ_h	viscous and thermal characteristic lengths
M_t, M_r	sensitivities of the transmitting and receiving microphones
p	pressure variation
P_0	static pressure
q_t	short-circuit volume velocity of the diaphragm of the transmitting microphone
R	outer radius of the slit
R_1	dimension of the annular cavity: inner radius
R_2	dimension of the annular cavity: outer radius
S	cross-section area of the cylindrical cavity
S_t, S_r	areas of the transmitting and receiving diaphragms
u_{r0}	open-circuit voltage of the receiving microphone
v_t, v_R	velocity fields of the transmitting and receiving diaphragms
$\underline{v_u}$, v_u	u-component of the particle velocity and its mean value across the domain considered (across the section of cylindrical cavity, tubes, or slits)
V	volume of the cylindrical cavity
x_t	coordinate along the axis of the tubes
Y^u_c	input acoustic admittance of the small component to be characterized, i.e. ratio of the volume velocity to the acoustic pressure ($u = s$ for the slit and $u = t$ for the tubes)
Y_t, Y_r	acoustic admittances of the transmitting and receiving microphones
Y_E, Y_T	electrical and acoustic transfer admittances when the element to be characterized is flush-mounted on the lateral wall of the cavity
Y^0_E, Y^0_T	electrical and acoustic transfer admittances when the cavity is totally closed
Y_{T0}	acoustic transfer admittance of the cavity having the flush-mounted element to be measured when the admittance of this element Y_c disappears
Z_L	acoustic impedance at the output of each tube
β	increase in pressure per unit increase in temperature at a constant density
$\gamma = C_P/C_V$	specific heat ratio
$\gamma_{\mu\nu}$	$(\nu+1)$th zero of the first derivative of the bessel function J_μ
ζ_{z0}, $\zeta_{z\ell}$	specific admittances of the walls of the cylindrical cavity at $z = 0$ and ℓ
η	bulk viscosity
λ	thermal conductivity
μ	shear viscosity
χ	complex wavenumber in the slit
χ_1, χ_2	complex wavenumbers in the annular cavity
ρ'	density variation
ρ_0	fluid density
σ	entropy variation
σ_c	input area of the element to be characterized
$\underline{\tau}$, τ	temperature variation and its mean value across the domain considered (across the section of the cylindrical cavity, tubes, or slits)

$\psi^d_{\mu v}$	cylindrical eigenfunctions	$J_n(x)$, $Y_n(x)$	Bessel, Neumann functions (order n)
ω	angular frequency		

behaviours have being extensively discussed in the literature (they are reported in many textbooks [2,3]): analytical modelling for each of these components and for their associations are provided, wherein viscosity, heat conduction, inertia, and compressibility of the gas are considered, beyond realistic boundary conditions (no slip conditions and no temperature variations near the walls). But the theoretical characteristics are usually obtained with a relative uncertainty greater than 50% (due to the geometrical uncertainties of these components).

Therefore, characterizing experimentally the input of these kinds of components (or their associations in the form of one-port passive linear acoustic systems), that is to say measuring their input impedance to control their behaviours with a good accuracy (i.e. with a relative uncertainty of the order of 10^{-2}) is of importance. It was very difficult, even impossible, until now, because their input impedance is usually much greater than those involved in the measuring set-ups. Such impedance measurement set-ups usually involve two linear transducers: one related to the pressure variation and the other to the volume velocity (the last one often being the source of energy described by its volume velocity). Even the calibration of the measurement set-up is conducted with the same coupling as for the measurement itself: it is not realistic, however, to try to obtain accurate results for practical use when using the techniques currently available (a review of these techniques is given in references [4,5]). Especially, this is true in the characterization of the input of such very small acoustic components over a wide frequency range (typically from 20 Hz to more than 20 kHz).

The question then arises: how can this measurement be achieved? To investigate this problem more closely, we consider the system illustrated schematically in Fig. 1. The cavity (the coupler) is a circular cylinder, closed at its ends by two electrostatic reciprocal transducers (electrostatic microphones): one used as a transmitter and the other as a receiver. The entrance of the small acoustic component to be measured is flush-mounted, localized on the lateral wall of the cavity (for the artificial ear, this cavity is the one of the artificial ears itself). Therefore, measuring the electrical transfer admittance between the input and the output of the device and modelling the acoustic transfer admittance of the cavity provide results which lead to the input impedance of the element to be measured. The measurement procedure benefits from the very well-established reciprocity calibration method and the corresponding set-up [6–9]. Therefore, the main purpose of the paper is to present the measurement method suggested here, the results obtained on typical elements used in many electroacoustic devices, and to discuss the precision that can be achieved. The example design for an artificial ear as specified in IEC 60318-1 provides a good example of a device containing the types of elements of interest, and has been the motivation for choosing the configurations to be studied here. Because the only way to discuss this

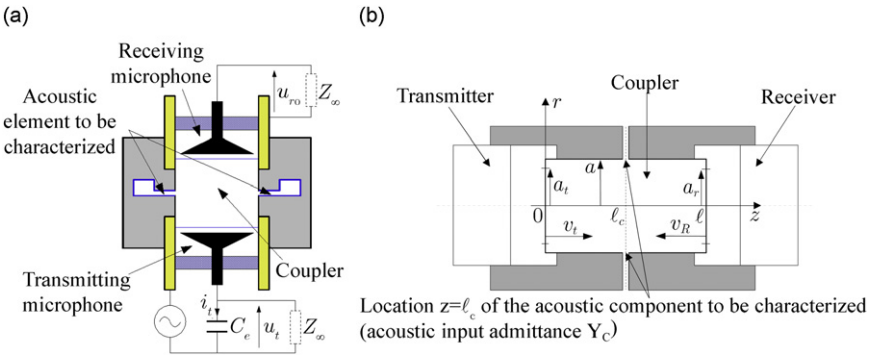

Fig. 1. (a) Measurement device, (b) Notations: a cylindrical cavity (coupler) of length ℓ and radius a, two transducers of radius a_t (transmitter) and a_r (receiver) located, respectively, at $z = 0$ and $z = \ell$.

precision is to compare the experimental results with the theoretical ones, appendices present the models that must be used in the frequency bandwidth 20 Hz–20 kHz.

2. The measurement method

2.1. The measurement methodology

The heart of the set-up comprises a cylindrical cavity (Fig. 1) filled with a gas (called the "coupler"). The length ℓ (5.111 or 4.639 mm) of the cavity has the same order of magnitude as its radius a (4.6504 mm), both being much greater than the boundary layer thicknesses so that approximation recalled in appendix (Eq. (A.20)) can be assumed in the analytical expression of the wave number (see Section 3). The cavity is closed at its ends by the diaphragms of two flush-mounted electrostatic transducers (electrostatic microphones): one being used as a transmitter (radius a_t) set at $z = 0$ and the other as a receiver (radius a_r) set at $z = \ell$. The radii a_t and a_r are smaller than the radius of the cavity but very close to it. The diaphragms of the transmitter and the receiver vibrate, respectively, at the velocity v_t (the velocity field of the transmitter diaphragm) and the velocity v_R (created by the acoustic pressure field on its membrane).

The input acoustic admittance Y_c to measure, defined as the ratio of the volume velocity to the acoustic pressure at the entrance of the element considered, is located on the lateral wall of the cavity at $z = \ell_c$ and $r = a$, on a small area denoted σ_c assumed to be much smaller than the total area of the lateral wall of the cylinder, separating the cavity into two parts. The quantities of interest [7] for the purpose are both the electrical transfer admittance Y_E and the acoustic transfer admittance Y_T. The electrical transfer admittance is defined as the ratio of the current i_t through the transmitting transducer to the open-circuit voltage u_{r0} of the receiving microphone:

$$Y_E = \frac{i_t}{u_{r0}}. \tag{1}$$

The acoustic transfer admittance is defined as the ratio of the short-circuit volume velocity q_t of the diaphragm of the transmitting microphone to the sound pressure $p(\ell)$ acting on the diaphragm of the receiving microphone,

$$Y_T = \frac{q_t}{p(\ell)}, \tag{2}$$

where the short-circuit volume velocity q_t of the diaphragm of the transmitting microphone is given by

$$q_t = S_t v_t + Y_t p(0), \tag{3}$$

where Y_t is the acoustic admittance of the transmitting transducer with $S_t = \pi a_t^2$.

The analytical expression of the acoustic transfer admittance denoted Y_T^0, for a totally closed coupler (cavity without a flush-mounted element on the lateral wall, i.e. $Y_c = 0$) [8,9] being known (see Section 3), measuring the corresponding electrical transfer admittance Y_E^0 leads to the value of the product of the pressure sensitivities of the electrostatic microphones [7]:

$$M_t M_r = \frac{Y_T^0}{Y_E^0}. \tag{4}$$

Then, measuring the electrical transfer admittance Y_E when the element to be characterized is flush-mounted on the lateral wall of the cavity gives the value of the acoustic transfer admittance

$$Y_T = M_t M_r Y_E, \tag{5}$$

or, substituting from Eq. (4),

$$Y_T = \frac{Y_T^0}{Y_E^0} Y_E. \tag{6}$$

Therefore, expressing Y_T as a function of the input acoustic admittance Y_c of the element to be characterized (see Section 3 below) allows obtaining the value of the unknown Y_c. In practice, the cavity used when the

element is flush-mounted is not exactly the same as the totally closed cavity (without the element). Actually, they are as close as possible to each other in order to make use of the same modelling for both cavities, with the same accuracy, and moreover the dimensions of each of them are measured carefully before they are inserted into the set-up. Finally, the measurement procedure benefits from the very well-optimized reciprocity calibration method and the corresponding set-up [6–9].

2.2. The reciprocity technique to measure the electrical transfer admittance

As mentioned in Section 2.1, the measured quantity is the electric transfer admittance in both cases, i.e. when the cavity is close (Y_E^0) and when the element to be characterized is flush mounted on the lateral wall of the cavity (Y_E), the acoustic transfer admittances Y_T^0 and Y_T being expressed analytically (see the next section). The procedure used for the measurements is the one given in the standard [7], which can be summarized as follows:

The electric transfer admittances Y_E^0 and Y_E defined by Eq. (1) are measured. The output open-circuit voltage u_{r0} is obtained using the insert voltage technique [7], and the input current i_t is deduced from the voltage developed across a series-connected capacitor $u_t = i_t/(\mathrm{j}\omega C_e)$ knowing the value of the capacitance C_e (Fig. 1a).

3. Analytical expression of the acoustic transfer admittance Y_T of the coupler

As mentioned in the previous section, the acoustic transfer admittance Y_T defined by Eqs. (2) and (3) must be expressed analytically as a function of both the acoustic pressure field inside the coupler (taking into account the effect of the viscous and thermal boundary layers) and the input admittance Y_c of the element flush-mounted on the lateral surface of the coupler. The accurate analytical modelling for the pressure fluctuations inside the cavity starts with the classical theory adapted to the purpose (Refs. [8–10], reported in Appendix A.1). It is worth noting that the viscous and thermal layer effects must be taken into account in order to derive benefit from the precision of the measurement using the reciprocity technique (0.01 dB, see Eq. (20) and the discussion at the end of paragraph 3).

Assuming both that the radii a_t and a_r are nearly equal to a and that the input admittance Y_c of the element leads to a pressure acoustic field which does not depend on the azimuthal coordinate θ, and then considering only a plane wave which travels back and forth along the z-axis of the cylindrical cavity, which does not depend on the r- and θ-coordinates, and which satisfies the viscous and thermal lateral boundary conditions, the set of equations which governs the acoustic pressure field takes the following form:

(i) Propagation equation [8] and Eq. (A.17):

$$\left(\frac{\partial^2}{\partial z^2} + k_z^2\right) p(z) = 0 \quad \text{for } 0 \leqslant z \leqslant \ell. \tag{7a}$$

In this equation, the complex axial wavenumber k_z accounts for the viscous and thermal boundary layer effects (see Appendix A). Thus, in the frequency range of interest (20 Hz, 20 kHz), it is given by, to the first-order approximation with respect to $\sqrt{k_0 \ell'_v}$ and $\sqrt{k_0 \ell_h}$ and assuming asymptotic behaviour (A.20) because $|k_{v,h} a| > 11$: in the frequency range of interest (20 Hz, 20 kHz)

$$k_z^2 \approx k_0^2 \left[1 + \frac{1-\mathrm{j}}{\sqrt{2}} \frac{2}{a\sqrt{k_0}} \left(\sqrt{\ell'_v} + (\gamma - 1)\sqrt{\ell_h}\right)\right] \tag{7b}$$

with $k_0 = \omega/c_0$ the adiabatic wavenumber, $\ell'_v = \mu/(\rho_0 c_0)$, and $\ell_h = \lambda/(\rho_0 c_0 C_P)$ the viscous and thermal characteristic lengths, μ and λ being, respectively, the shear viscosity coefficient and the coefficient of thermal conductivity. Note that the characteristic lengths are approximately equal, respectively, to $\ell'_v \approx 4.5 \times 10^{-8}$ m and $\ell_h \approx 6 \times 10^{-8}$ m for air under usual conditions.

(ii) Boundary condition at $z = 0$ [8]:

$$S v_z = S v_t - Y_b p \quad \text{at } z = 0, \tag{8a}$$

where Y_b is the thermal boundary layer admittance (to the first-order approximation with respect to $\sqrt{k_0\ell_h}$) [2,3,8]:

$$Y_b \approx \frac{S}{\rho_0 c_0}\frac{1+\mathrm{j}}{\sqrt{2}}\sqrt{k_0}(\gamma-1)\sqrt{\ell_h} \tag{8b}$$

and where, inserting Eq. (A.19) into Eq. (A.10):

$$Sv_z(z) = -\frac{1}{Z_v}\frac{\partial}{\partial z}p(z) \tag{8c}$$

with $S=\pi a^2$,

$$Z_v = \frac{1}{S}\frac{\mathrm{j}k_0\rho_0 c_0}{1-K_v}, \quad K_v = \frac{2}{k_v a}\frac{J_1(k_v a)}{J_0(k_v a)} \quad \text{and} \quad k_v = \frac{1-\mathrm{j}}{\sqrt{2}}\sqrt{k_0/\ell'_v}. \tag{8d}$$

It is worth noting that Eq. (8c) is the Euler equation which includes the viscous boundary layer effects as we can see as follows: in the frequency range of interest, the modulus of $(k_v a)$ is always much greater than unity ($|k_v a|>13$). Therefore, function K_v can be asymptotically approximated by

$$K_v \approx \frac{1-\mathrm{j}}{\sqrt{2}}\frac{2}{a}\sqrt{\frac{\ell'_v}{k_0}} \tag{9}$$

leading to [Eq. (8c)]

$$-\frac{\partial}{\partial z}p \approx \mathrm{j}k_0\rho_0 c_0\left[1+\frac{1-\mathrm{j}}{\sqrt{2}}\frac{2}{a}\sqrt{\frac{\ell'_v}{k_0}}\right] \tag{10}$$

when the modulus of the last factor $([2/a]\sqrt{\ell'_v/k_0})$ takes values between 0.15 (20 Hz) and 5×10^{-3} (20 kHz). This last factor is not negligible in the lower frequency range.

(iii) Boundary condition at $z=\ell$ [8]:

$$Sv_z = (Y_b + Y_r)p \quad \text{at } z=\ell, \tag{11}$$

where $Y_r = Sv_R/p(\ell)$ is the acoustic admittance of the receiving microphone.

(iv) Boundary condition at $r=a$, $z=\ell_c$ (volume velocity conservation law and acoustic pressure continuity at the input of the element to be measured):

$$Sv_z(\ell_c^-) = Sv_z(\ell_c^+) + Y_c p(\ell_c), \tag{12a}$$

$$p(\ell_c^-) = p(\ell_c^+) = p(\ell_c), \tag{12b}$$

where $Sv_z(\ell_c^+)$ and $Sv_z(\ell_c^-)$ being, respectively, the volume velocity in the upper and the lower part of the coupler at $z=\ell_c$.

(v) Full expression for the solution

The expressions for the complex amplitudes of the plane wave solutions of Eq. (7a) in each domain of the coupler ($z<\ell_c$ and $z>\ell_c$), respectively, subject to the boundary conditions (8a) and (11), both satisfying the interface conditions (12a), when the time-periodic source activity is given by the harmonic ($\mathrm{e}^{\mathrm{j}\omega t}$) volume velocity ($Sv_t$) of the transmitting transducer ($z=0$), are written, respectively, as

$$p(z) = A(\mathrm{e}^{-\mathrm{j}k_z z} + B\mathrm{e}^{\mathrm{j}k_z z}) \quad \text{for } 0\leqslant z\leqslant \ell_c, \tag{13a}$$

$$p(z) = C(\mathrm{e}^{-\mathrm{j}k_z z} + D\mathrm{e}^{\mathrm{j}k_z z}) \quad \text{for } \ell_c\leqslant z\leqslant \ell. \tag{13b}$$

The integration constants A, B, C, and D are obtained from the boundary conditions (8a) and (11), and the interface conditions (12a,b). They are given in Appendix C.

(vi) The acoustic transfer admittance of the cavity

Applying expressions (13a, b) for the acoustic pressure, the acoustic transfer admittance Y_T (which is the quantity of interest for the measurement of the admittance Y_c) given by Eqs. (2) and (3), namely

$$Y_T = \frac{Sv_t + Y_t p(0)}{p(\ell)} \tag{14}$$

takes the following form:

$$Y_T = Y_{T0} + \alpha Y_c, \tag{15}$$

where

$$\alpha = \frac{1}{2}\left[\mathrm{j}\frac{Y_t + Y_r + 2Y_b}{Y_i}\sin k_z\ell + \left(1 + \frac{(Y_t + Y_b)(Y_r + Y_b)}{Y_i^2}\right)\cos k_z\ell \right.$$
$$\left. +\mathrm{j}\frac{Y_r - Y_t}{Y_i}\sin k_z(\ell - 2\ell_c) + \left(1 - \frac{(Y_t + Y_b)(Y_r + Y_b)}{Y_i^2}\right)\cos k_z(\ell - 2\ell_c)\right] \tag{16}$$

with

$$Y_i = \frac{\pi a^2}{\rho_0 c_0}\sqrt{[1 + (\gamma - 1)K_h](1 - K_v)}, \tag{17a}$$

$$Y_i \approx \frac{\pi a^2}{\rho_0 c_0}\left[1 + \frac{1 - \mathrm{j}}{\sqrt{2}}\frac{2}{a\sqrt{k_0}}(-\sqrt{\ell'_v} + (\gamma - 1)\sqrt{\ell_h})\right] \tag{17b}$$

and where

$$Y_{T0} = \left[Y_i + \frac{(Y_t + Y_b)(Y_r + Y_b)}{Y_i}\right]\mathrm{j}\sin k_z\ell + (Y_t + Y_r + 2Y_b)\cos k_z\ell \tag{18}$$

is the acoustic transfer admittance of the cavity having the flush-mounted element to be measured when its admittance Y_c disappears.

Combining Eqs. (6) and (15) to remove the admittance Y_T leads to the following expression of the acoustic input admittance Y_c of the component:

$$Y_c = \frac{Y_T^0}{\alpha}\left(\frac{Y_E}{Y_E^0} - \frac{Y_{T0}}{Y_T^0}\right), \tag{19}$$

where Y_{T0} is given by Eq. (18), ℓ being the length of the cavity with the element to be measured, and Y_T^0 is given by the same equation, ℓ being the length of the totally closed cavity (see the discussion at the end of Section 2), and where the measured quantities Y_E^0 and Y_E are, respectively, related to the totally closed cavity and the cavity with the element to be measured.

Note that in the lower frequency range, roughly up to around 2 kHz, i.e. when the dimensions of the cavity are much lower than the acoustic wavelength ($|k_z\ell| \ll 1$), it is justified to retain the first order in the factor $k_z\ell$ in expression (15) of Y_T and to use the approximate expressions (8b), (7b), and (17b) for Y_b, k_z, and Y_i, respectively, yielding the result [2,3,8,11]:

$$Y_T \approx \mathrm{j}\omega\frac{V}{\gamma P_0}\left[1 + (\gamma - 1)\frac{\mathscr{A}}{V}\frac{1 - \mathrm{j}}{\sqrt{2}}\sqrt{\frac{\ell_h}{k_0}}\right] + Y_t + Y_r + Y_c, \tag{20}$$

where the ratio of the total area of the surface of the cavity to its volume is $\mathscr{A}/V = 2/a + 2/\ell$ (this last result is directly demonstrated in the appendix of Ref. [8] when $Y_c = 0$). The acoustic admittance $\mathrm{j}\omega V/(\gamma P_0)$ (the first term of Eq. (20)) represents the purely reactive admittance of the (small) cavity when its dimensions are much lower than the acoustic wavelength, assuming perfectly rigid boundaries.

It is worth noting that detecting a variation reaching 0.01 dB [7] between measurements with and without an element to be measured means detecting a relative variation of Y_T given by

$$20\log\left(\frac{Y_T + \Delta Y_T}{Y_T}\right) \approx 0.01\,\mathrm{dB}, \quad \text{i.e. } \frac{\Delta Y_T}{Y_T} \approx 10^{-3}.$$

To be able to obtain the value of the unknown admittance Y_c with approximately two significant figures, the ratio $|Y_c|/(\omega V/(\gamma P_0))$ must be greater than 10×10^{-3}, i.e. $|Y_c| > 3 \times 10^{-14}\omega$, that is for example at 100 Hz $|Y_c| > 2 \times 10^{-11}\,\mathrm{m^3\,s^{-1}\,Pa^{-1}}$. On the other hand, one can say that the effect of heat conduction (second term in

Eq. (20)) and the effects of the transducers represented by their admittances Y_t and Y_r are non-negligible because, respectively:

$$(\gamma - 1)\frac{\mathscr{A}}{V}\sqrt{\frac{\ell_h}{k_0}} \approx 0.06 \quad \text{at } 100\,\text{Hz}$$

and, for the microphones used (B&K Type 4180),

$$\frac{|Y_t| + |Y_r|}{\omega V/(\gamma P_0)} \approx 0.07,$$

in the lowest frequency range.

Remark. It is noteworthy that when the input admittance Y_c of the element leads to a pressure acoustic field which depends on the azimuthal coordinate θ, the plane wave approximation fails. A more sophisticated behaviour of the acoustic pressure field must be considered. A model, presented in Appendix B, has been developed when elements are flush-mounted on the lateral wall of the cavity, which is an extension of the model given in the literature [9] for the totally closed cavity (without an element on the lateral surface of the cavity).

4. Theoretical and experimental results, discussion

With respect to the efficiency of the method, in this section we present the input admittance Y_c of components flush-mounted on the lateral wall of the coupler as a function of the frequency in the frequency range (20 Hz, 20 kHz).

To validate the measurement method and evaluate its accuracy, two basic acoustic elements, derived from the design of the artificial ear, have been selected. These were chosen on the basis that they can be modelled accurately as well as studied experimentally. The first one is a thin, short annular slit open at its end on a free space (Fig. 2) (its acoustic input admittance does not depend on the θ-coordinate). The second one is a set of four thin, short cylindrical tubes which are placed at the azimuthal coordinates $\theta = 0, \pi/2, \pi, 3\pi/2$ in order to ensure a behaviour of the field in the coupler such that the modes considered can only be those which do not depend on the θ-coordinate (Fig. 3). These four tubes are loaded at their output either by a free field or by the field in a closed small annular cavity. The analytical modelling of these components, providing accurate expressions of their input acoustic admittances, is presented in Appendices D and E.

The experimental values of Y_c are obtained from the measurement of both the electrical transfer admittance Y_E^0 of the totally closed coupler and the electrical transfer admittance Y_E of the coupler with a component on the lateral wall, using Eq. (19) to relate the unknown Y_c to these admittances (the parameters Y_{T0}, Y_T^0, and α being known, Eqs. (18) and (16), respectively). The theoretical values of Y_c are derived from expressions (D.6), (E.3), and (E.2), respectively for an annular slit open in a free space at the end (Fig. 4), for a set of four tubes either open in a free space (Fig. 5) or closed by an annular cavity (Fig. 6) (the input impedance of this annular cavity being given by Eq. (E.8)).

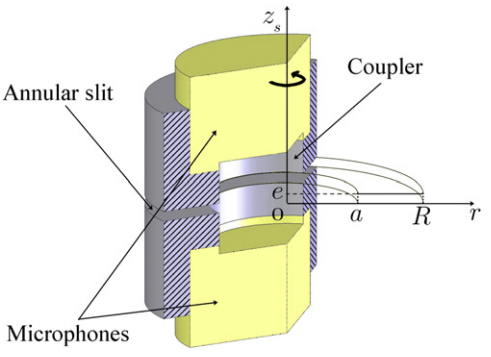

Fig. 2. Annular slit.

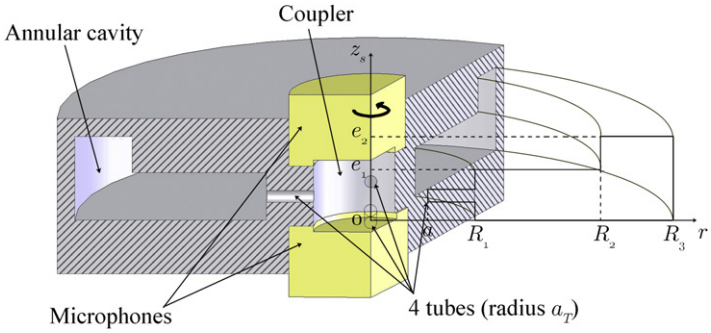

Fig. 3. Four tubes connected to an annular cavity.

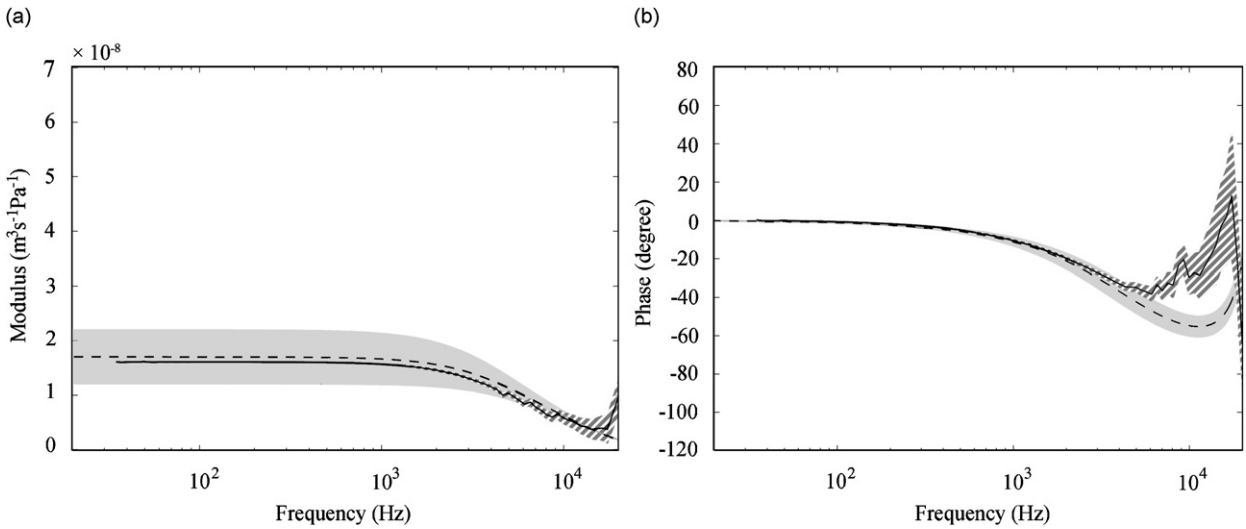

Fig. 4. Acoustic input admittance of an annular slit, (a) modulus and (b) phase, experimental and theoretical results and uncertainties: (- - -) theoretical admittance, (——) experimental admittance, (shared area) uncertainty interval on the theoretical admittance, (hatched area) uncertainty interval on the experimental admittance.

The dimensions of the slit, the tubes, and the annular cavity are given, respectively, in Tables 1–3.

Two values are given in Table 2 for the radii of the tubes. One is the manufacturer's data and the other is from our own measurements (of only the end of the tube), using a microscope.

Expression (20) for the acoustic transfer admittance, accurate in the lower frequency range (approximately 20 Hz–5 kHz), shows significant deviations from the more sophisticated model presented in Appendix B in the upper frequency range (beyond about 5 kHz), as presented and discussed in detail in Ref. [9]. The discrepancies observed at these frequencies in Figs. 4–6 may be due to the fact that the relevance of the model used here (Eq. (20)) to calculate the acoustic transfer admittances occurs only up to 5 kHz.

In Fig. 4, which shows the acoustic input impedance of an annular slit, the theoretical uncertainties (shaded areas) have been calculated using the values of the uncertainties on the thickness and the length given in Table 1, and the experimental uncertainties (hatched area) are derived from the lack of reproducibility of the measurement in the highest frequency range (beyond 2 kHz).

In Figs. 5 and 6, which show the input admittance of a set of four tubes, respectively, open on a free space or closed by an annular cavity, we must draw attention to the discrepancies between the theoretical results obtained using the values of the radii given by the manufacturer and those obtained with our own measurements: they provide an explanation for the lack of accuracy between the two theoretical results on the

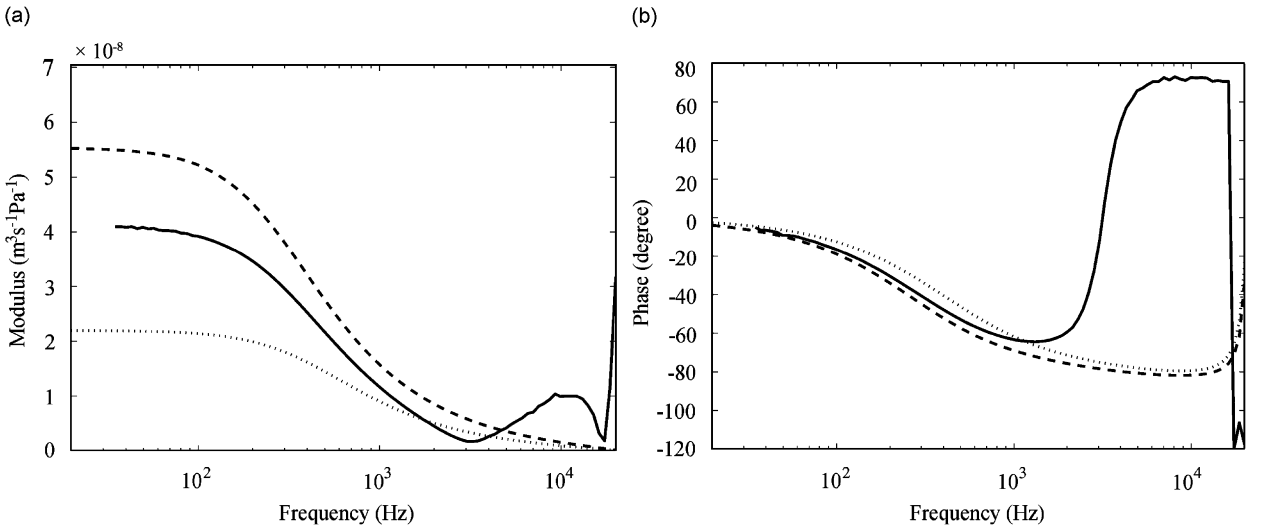

Fig. 5. Acoustic input admittance of four open tubes, (a) modulus and (b) phase, experimental and theoretical results: (——) experimental admittance, (- - -) theoretical admittance (manufacturer data), (· · · · ·) theoretical admittance (our own measurements).

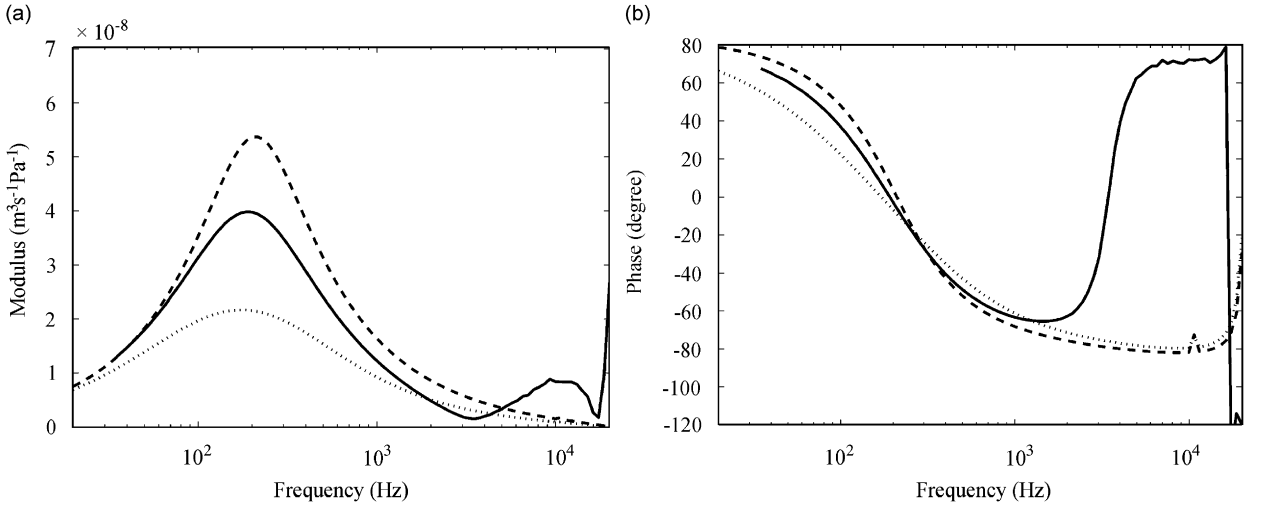

Fig. 6. Acoustic input admittance of four tubes connected to a cavity, (a) modulus and (b) phase, experimental and theoretical results: (——) experimental admittance, (- - -) theoretical admittance (manufacturer data), (· · · · ·) theoretical admittance (our own measurements).

Table 1
Dimensions and associated uncertainties of the annular slit

	Dimension (μm)	Uncertainty (μm)
Thickness	71.2	6
Length	3.883×10^3	6

one hand and between the experimental result and each theoretical result on the other (the experimental result being fortunately between the theoretical ones).

The results presented above make use of slits and tubes used in classical devices. In order to show that there is a close agreement between the analytical and experimental results (up to several kHz), a set of four tubes has been designed with a very high accuracy: all of them have a radius of 225 μm with an uncertainty lower than

Table 2
Dimensions and associated uncertainties of the four cylindrical tubes

	Dimension (μm)	Uncertainty (μm)
Radii (manufacturer data)	225	10
Radii (our own measurements)	190 ; 185 ; 180 ; 150	8 ; 23 ; 20 ; 30
Length	3.800×10^3	50

Table 3
Dimensions and associated uncertainties of the annular cavity

	Dimension (μm)	Uncertainty (μm)
Radius R_1	8.446×10^3	3
Radius R_2	20.526×10^3	3
Radius R_3	24.068×10^3	3
Thickness e_1	4.082×10^3	6
Thickness e_2	7.150×10^3	6
Volume	$8053\,\text{mm}^3$	$50\,\text{mm}^3$

Table 4
Dimensions and associated uncertainties of the four cylindrical tubes (high-accuracy device)

	Dimension (μm)	Uncertainty (μm)
Radii	225	1
Length	3.800×10^3	10

1 μm and a length of 3.8 mm with an uncertainty lower than 10 μm (Table 4). The results obtained are shown in Fig. 7: the experimental and theoretical results are in very good agreement up to 5 kHz (the uncertainties are around 1% for the modulus and 1 degree for the phases), showing that the method permits the experimental characterization of the input behaviour of such components with a good accuracy.

5. Conclusion

The original motivation for this study was to characterize the input impedance of small slits or tubes (or their associations in the form of one-port passive linear acoustic systems). The small elements used until now can be described with a refinement that is consistent with the requirement of the devices which contain them (artificial ear, loudspeakers, microphones, and most acoustic devices). But the sensitivity of the theoretical results to uncertainties in the thickness (slits) or diameter (tubes) of these elements is not negligible (the uncertainties in the admittance can reach 90% of the value expected for the input admittance). Therefore, nowadays, accurate experimental results for the input admittance Y_c of these small elements not available until now are required to optimize the behaviour of acoustic devices as for example the artificial ear. Moreover, acoustic devices that will be miniaturized in the future, using MEMS techniques, would require appropriate measurements of extremely miniaturized slits and tubes because the limit of validity of the classical theory reported in this paper could be exceeded while diminishing the dimensions of the elements, and then the theoretical analysis would be ambiguous.

Therefore, the main purpose of the paper is to put forward ideas to measure the input admittance of small slits and tubes, derived from the reciprocity calibration method, using, for example, commercially available equipment on the market, and to convey our conviction that this technique would provide accurate measurements of these input admittances up to several kHz, because a significant precision can be achieved.

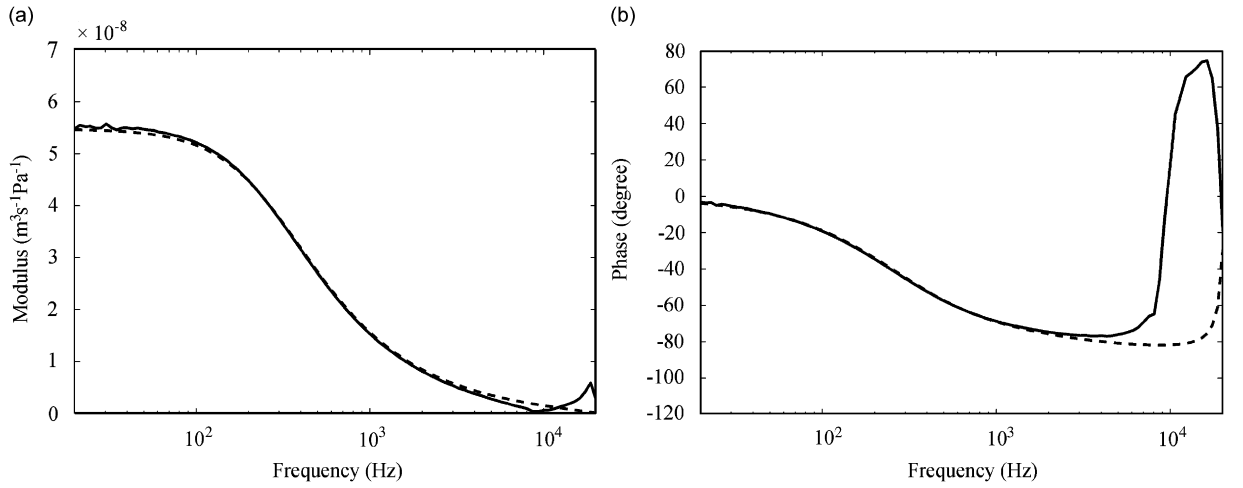

Fig. 7. Acoustic input admittance of four open tubes (high-accuracy device), (a) modulus and (b) phase, experimental and theoretical results: (——) experimental admittance, (- - -) theoretical admittance.

The validation of the method would require theoretical investigations that are consistent with the precision needed to achieve such measurements. As mentioned above, suitable modelling is available in the literature, but it appears that the uncertainties in the results calculated prevent us from validating definitely the experimental method, the dominant source of uncertainties in the magnitude and in the phase in the calculated admittances being the uncertainties in the thickness or the radius of the small elements. Therefore, the validation of the experimental method implies to design small components (here tubes) with a very high precision, namely 1 μm in place of roughly 10 μm; with these refinements of the machining of the tubes, the results calculated provide this validation.

Then, the experimental results show that the method of measurement presented in this paper will be adequate to access the input behaviour of such small components with a good precision, supplanting the theoretical results which are not accurate for the usual small components. This is important in practice when using the acoustic method for accurate measurements, for example the measurement of the Boltzmann constant with a relative uncertainty of 10^{-6} [1]. Also, this measurement method can be useful to improve our knowledge about the acoustic behaviour of each component of the artificial ear (among other applications) and thus to propose theoretical models more accurate than those currently used [12].

Appendix A. Propagation equation in thermo-viscous fluid-filled tubes and slits: quasi-plane wave approximation [2,3,8–10]

A.1. General formulation

The variables describing the dynamic and thermodynamic states of the fluid are the pressure variation p, the particle velocity $\underline{\mathbf{v}}$, the density variation ρ', the entropy variation σ, and the temperature variation $\underline{\tau}$ (the reason why $\underline{\mathbf{v}}$ and $\underline{\tau}$ are underlined appears hereafter, Eq. (A.9)). The parameters which specify the properties and the nature of the fluid are the ambient values of the density ρ_0, the static pressure P_0, the shear viscosity coefficient μ, the bulk viscosity coefficient η, the coefficient of thermal conductivity λ, the specific heat coefficient at constant pressure and constant volume per unit of mass C_P and C_V, respectively, the specific heat ratio γ, and the increase in pressure per unit increase in temperature at constant density β. A complete set of linearized homogeneous equations governing small-amplitude disturbances of the fluid includes the following:

- The Navier–Stokes equation

$$\frac{1}{c_0}\frac{\partial \underline{\mathbf{v}}}{\partial t} + \frac{1}{\rho_0 c_0}\nabla p = \ell_v \nabla(\nabla \cdot \underline{\mathbf{v}}) - \ell'_v \nabla \times (\nabla \times \underline{\mathbf{v}}), \tag{A.1}$$

where the characteristic lengths ℓ_v and ℓ'_v are defined by

$$\ell_v = \frac{\eta + 4/3\mu}{\rho_0 c_0} \quad \text{and} \quad \ell'_v = \frac{\mu}{\rho_0 c_0}.$$

- The conservation of mass equation, taking into account the thermodynamic law expressing the density variation as a function of the independent variables p and $\underline{\tau}$,

$$\rho_0 c_0 \nabla \cdot \underline{\mathbf{v}} + \frac{\gamma}{c_0}\frac{\partial}{\partial t}(p - \beta \underline{\tau}) = 0. \tag{A.2}$$

- The Fourier equation for heat conduction, taking into account the thermodynamic law expressing the entropy variation as a function of the independent variables p and $\underline{\tau}$,

$$\left(\frac{1}{c_0}\frac{\partial}{\partial t} - \ell_h \nabla^2\right)\underline{\tau} = \frac{\gamma - 1}{\beta\gamma}\frac{1}{c_0}\frac{\partial p}{\partial t}, \tag{A.3}$$

where $\ell_h = \lambda/(\rho_0 c_0 C_P)$.

The boundary surfaces of the domain are assumed to be locally plane. The local coordinates $(u, \mathbf{w})$ can then be used, where u is the coordinate normal to the boundary inwardly directed, with $u = s$ on the boundary, and where $\mathbf{w} = (w_1, w_2)$ is the couple of coordinates tangential to the boundary.

The acoustic field inside the domain considered should be the solution of this set of three equations with the requirement of regular behaviour at the centre if the domain is cylindrical, and with the boundary conditions at the surface of the domain: the normal and tangential components of the particle velocity and the temperature variation disappear on the boundary, namely

$$\underline{v}_u = \underline{v}_{w_1} = \underline{v}_{w_2} = 0 \quad \text{and} \quad \underline{\tau} = 0 \ \text{at} \ u = s. \tag{A.4}$$

Furthermore, several hypotheses can be made here considering the solutions near the boundaries. These assumptions can be summarized as follows:

- the normal component of the particle velocity $\underline{v}_u$ is much smaller than the tangential components $\underline{v}_{w_1}$ and $\underline{v}_{w_2}$,
- the spatial derivative of the temperature variation $\underline{\tau}$ and of the w_i-component of the particle velocity $\underline{v}_{w_i}$ with respect to the coordinate w_i, in the Fourier equation and in the Navier–Stokes equation, respectively, are much smaller than the derivatives with respect to the u-coordinate.

These approximations enable us to simplify the expressions of Eqs. (A.1) and (A.3) near the boundaries as follows (for harmonic motion, $e^{j\omega t}$):

$$\left(1 + \frac{1}{k_v^2}\frac{\partial^2}{\partial u^2}\right)\underline{\mathbf{v}}_w = -\frac{1}{j\omega\rho_0 c_0}\nabla_w p, \quad (u - s) \geqslant 0, \forall \mathbf{w} \tag{A.5a}$$

with

$$k_v = \frac{1 - j}{\sqrt{2}}\sqrt{\ell'_v / k_0} \tag{A.5b}$$

and Eq. (A.3) gives

$$\left(1 + \frac{1}{k_h^2}\frac{\partial^2}{\partial u^2}\right)\underline{\tau} = \frac{\gamma - 1}{\beta\gamma}p, \quad (u - s) \geqslant 0, \forall \mathbf{w} \tag{A.6a}$$

with

$$k_h = \frac{1-\mathrm{j}}{\sqrt{2}}\sqrt{\ell_h/k_0}. \tag{A.6b}$$

The quasi-plane wave approximation assumes that the acoustic pressure field does not vary significantly with the variable u in the viscous and thermal boundary layers, near the walls. On the other hand, due to the viscous boundary layer, the **w**-components $\underline{\mathbf{v}}_w$ of the particle velocity depend strongly on the coordinate u inside this layer. Then the right-hand side of Eq. (A.5a) can be assumed to be quasi-independent of the u-coordinate, leading to the approximate solution of this equation, subject to the boundary condition $\underline{v}_u = 0$ at $u = s$, for a harmonic motion (the factor $\mathrm{e}^{\mathrm{j}\omega t}$ is omitted):

$$\underline{\mathbf{v}}_w = -\frac{1}{\mathrm{j}\omega\rho_0}\nabla_w p\left[1 - \frac{\Phi(-\mathrm{j}k_v u)}{\Phi(-\mathrm{j}k_v s)}\right], \tag{A.7}$$

where $\Phi(-\mathrm{j}k_v u)$ is the general solution of a homogeneous equation associated with Eq. (A.5a). In the same manner the solution $\underline{\tau}$ of Eq. (A.6a), subject to the boundary condition $\underline{\tau} = 0$ at $u = s$, is given by

$$\underline{\tau} = \frac{\gamma-1}{\beta\gamma}p\left[1 - \frac{\Phi(-\mathrm{j}k_h u)}{\Phi(-\mathrm{j}k_h s)}\right]. \tag{A.8}$$

Moreover, when considering a quasi-plane wave approximation, the effect of the viscous and thermal boundary layers given by these solutions can be approximated by their mean values across the domain considered (across the section of cylindrical cavities, tubes, or slits), neglecting that the pressure variation p depends on the coordinates over this section. Then the approximate solutions for the **w**-components of the particle velocity (denoted $\underline{\mathbf{v}}_w$) and for the temperature variation (denoted τ) reduce, respectively, to:

$$\underline{\mathbf{v}}_w \approx \frac{\mathrm{j}}{k_0\rho_0 c_0}\nabla_w p(u,\mathbf{w})\frac{1}{S_d}\iint_{S_d}\left[1 - \frac{\Phi(-\mathrm{j}k_v u)}{\Phi(-\mathrm{j}k_v s)}\right]\mathrm{d}S_d \tag{A.9}$$

$$\approx \frac{\mathrm{j}}{k_0\rho_0 c_0}\nabla_w p(u,\mathbf{w})[1 - K_v] \tag{A.10}$$

with

$$K_v = \left\langle\frac{\Phi(-\mathrm{j}k_v u)}{\Phi(-\mathrm{j}k_v s)}\right\rangle \tag{A.11}$$

and

$$\tau = \frac{\gamma-1}{\beta\gamma}p(u,\mathbf{w})[1 - K_h] \tag{A.12}$$

with

$$K_h = \left\langle\frac{\Phi(-\mathrm{j}k_h u)}{\Phi(-\mathrm{j}k_h s)}\right\rangle. \tag{A.13}$$

Combining Eqs. (A.10) and (A.12) with the mean value across the section of the domain of Eq. (A.2), and assuming that the u-component of the particle velocity v_u is given by the usual Euler equation

$$v_u = \frac{\mathrm{j}}{k_0\rho_0 c_0}\frac{\partial}{\partial u}p(u,\mathbf{w}) \tag{A.14}$$

leads finally to

$$\left[\frac{\partial^2}{\partial u^2} + (1 - K_v)\nabla_{\vec{w}}^2 + k_0^2(1 + (\gamma-1)K_h)\right]p = 0. \tag{A.15}$$

A.2. Application to cylindrical tubes (coupler and narrow tubes) and slits

(i) For a cylindrical cavity of radius a, the coordinates are:

$$u = a - r, \quad \mathbf{w} = (\theta, z). \tag{A.16}$$

Assuming that the propagation along the z-axis of the quasi-plane wave does not depend on the coordinates r and θ, Eq. (A.15) reduces to

$$\left[\frac{\partial^2}{\partial z^2} + k_z^2\right] p(z) = 0, \tag{A.17}$$

where

$$k_z^2 = k_0^2 \frac{1 + (\gamma - 1)K_h}{1 - K_v} \tag{A.18}$$

with $k_0 = \omega/c_0$ and

$$K_{v,h} = \frac{2}{k_{v,h}a} \frac{J_1(k_{v,h}a)}{J_0(k_{v,h}a)}. \tag{A.19}$$

Moreover, assuming that the radius a justifies approximating k_z asymptotically ($k_{v,h}a \gg 1$) gives the well-known result:

$$k_z^2 \approx k_0^2 \left[1 + \frac{1 - \mathrm{j}}{\sqrt{2}} \frac{2}{a\sqrt{k_0}} (\sqrt{\ell_v'} + (\gamma - 1)\sqrt{\ell_h})\right]. \tag{A.20}$$

(ii) For an annular slit of thickness e, the coordinates are $u = z_s$ or $u = e - z_s$, $\mathbf{w} = (r, \theta)$.
Assuming that the propagation occurs only along the r-axis and that the wave does not depend on the coordinates z_s and θ, Eq. (A.15) reduces to

$$\left[\frac{\partial^2}{\partial r^2} + \frac{1}{r}\frac{\partial}{\partial r} + \chi^2\right] p(r) = 0, \tag{A.21}$$

where

$$\chi^2 = k_0^2 \frac{1 + (\gamma - 1)K_h}{1 - K_v}, \quad \mathrm{Re}(\chi) > 0 \text{ and } \mathrm{Im}(\chi) < 0 \tag{A.22}$$

with

$$K_{v,h} = \frac{\tan(k_{v,h}e/2)}{k_{v,h}e/2}. \tag{A.23}$$

Appendix B. Modal solution for the sound pressure in the coupler

When the input admittance Y_c of the element to be measured, flush-mounted on the lateral wall of the cylindrical coupler, leads to a pressure acoustic field which depends on the azimuthal coordinate θ, the plane wave approximation (Eq. (A.17)) fails. It is the aim of this section to present a model describing this more sophisticated behaviour of the acoustic pressure field that must be considered (this model is an extension of the model given in Ref. [9]).

In this situation, the propagation Eq. (A.15) takes the following form (assuming that the spatial derivatives of the pressure variation p with respect to the r- and θ-coordinates are much lower than the derivative with respect to the z-coordinate):

$$\left[\frac{1}{r}\frac{\partial}{\partial r} r \frac{\partial}{\partial r} + \frac{1}{r^2}\frac{\partial^2}{\partial \theta^2} + \frac{\partial^2}{\partial z^2} + k^2\right] p(r, \theta, z) = 0, \tag{B.1}$$

where the expression of the wavenumber k is given by the right-hand side of Eq. (A.18)

$$k^2 = k_0^2 \frac{1+(\gamma-1)K_h}{1-K_v}, \tag{B.2}$$

where K_v and K_h being given by Eq. (A.19), or, to the first-order approximation with respect to $\sqrt{k_0\ell'_v}$ and $\sqrt{k_0\ell_h}$ (Eq. (A.20))

$$k^2 \approx k_0^2\left[1+\frac{1-\mathrm{j}}{\sqrt{2}}\frac{2}{a\sqrt{k_0}}(\sqrt{\ell'_v}+(\gamma-1)\sqrt{\ell_h})\right], \tag{B.3}$$

where this complex wavenumber k accounts for the viscous and thermal boundary layers on the lateral wall, in the framework of the quasi-plane wave approximation.

The problem addressed here is given by the propagation Eq. (B.1) associated with the following boundary conditions:

$$v_r = 0, \quad r=a, \ \ \theta\in(0,2\pi), \ \ z\in(0,\ell), \tag{B.4a}$$

$$v_r = \frac{Y_c}{\sigma_c}p, \quad r=a, \ \ \theta\in(0,2\pi), \ \ z=\ell_c, \tag{B.4b}$$

the input area σ_c of the element (whose acoustic admittance Y_c is the unknown to be measured here) being much smaller than the total lateral area of the cylinder,

$$\rho_0 c_0 v_z = \rho_0 c_0 v_t - \zeta_{z0}p, \quad r\in(0,a_t), \ \ \theta\in(0,2\pi), \ \ z=0, \tag{B.4c}$$

$$\rho_0 c_0 v_z = -\rho_0 c_0 v_R + \zeta_{z\ell}p, \quad r\in(0,a_r), \ \ \theta\in(0,2\pi), \ \ z=\ell, \tag{B.4d}$$

$$\rho_0 c_0 v_z = -\zeta_{z0}p, \quad r\in(a_t,a), \ \ \theta\in(0,2\pi), \ \ z=0, \tag{B.4e}$$

$$\rho_0 c_0 v_z = \zeta_{z\ell}p, \quad r\in(a_r,a), \ \ \theta\in(0,2\pi), \ \ z=\ell, \tag{B.4f}$$

where the specific admittances ζ_{z0} and $\zeta_{z\ell}$ express the viscous and the thermal boundary layer effects on the walls at $z=0$ and $z=\ell$.

On using notation (A.19) and applying, respectively, Eqs. (A.10) and (A.15), the boundary conditions (B.4a–f) can be written to the first order of the small quantities ζ_{z0} and $\zeta_{z\ell}$ (and for any value of $\theta\in(0,2\pi)$),

$$\frac{\partial p}{\partial n} = \frac{\partial p}{\partial r} = 0, \quad r=a, \ \ z\in(0,\ell), \tag{B.5a}$$

$$\frac{\partial p}{\partial n} = \frac{\partial p}{\partial r} = -\mathrm{j}k_0\rho_0 c_0 \frac{Y_c}{\sigma_c}p, \quad r=a, \ \ z=\ell_c, \tag{B.5b}$$

$$\frac{\partial p}{\partial n} = -\frac{\partial p}{\partial z} = \frac{\mathrm{j}k_0\rho_0 c_0}{1-K_v}v_z \approx \frac{\mathrm{j}k_0\rho_0 c_0}{1-K_v}v_t - \mathrm{j}k_0\zeta_{z0}p, \quad r\in(0,a_t), \ \ z=0, \tag{B.5c}$$

$$\frac{\partial p}{\partial n} = \frac{\partial p}{\partial z} = -\frac{\mathrm{j}k_0\rho_0 c_0}{1-K_v}v_z \approx \frac{\mathrm{j}k_0\rho_0 c_0}{1-K_v}v_R - \mathrm{j}k_0\zeta_{z\ell}p, \quad r\in(0,a_r), \ \ z=\ell, \tag{B.5d}$$

$$\frac{\partial p}{\partial n} = -\frac{\partial p}{\partial z} = -\mathrm{j}k_0\zeta_{z0}p, \quad r\in(a_t,a), \ \ z=0, \tag{B.5e}$$

$$\frac{\partial p}{\partial n} = \frac{\partial p}{\partial z} = -\mathrm{j}k_0\zeta_{z\ell}p, \quad r\in(a_r,a), \ \ z=\ell. \tag{B.5f}$$

The set of Eqs. (B.1) and (B.5a)–(B.5f), while appropriate for addressing the acoustic pressure field in the coupler, is in the following expressed in using the integral formulation as presented in Ref. [9, Section 2.3]. The main results are reported below, taking into account here the acoustic impedance Y_c of the element to be characterized, with a Green function satisfying at the cavity walls the same admittance boundary conditions as

the acoustic pressure p but homogeneous, namely:

$$\frac{\partial}{\partial n}G(\mathbf{r},\mathbf{r}_0) = -\mathrm{j}k_0\zeta_{z0}G(\mathbf{r},\mathbf{r}_0), \quad r\in(0,a),\ \ \theta\in(0,2\pi),\ \ z=0, \tag{B.6a}$$

$$\frac{\partial}{\partial n}G(\mathbf{r},\mathbf{r}_0) = -\mathrm{j}k_0\zeta_{z\ell}G(\mathbf{r},\mathbf{r}_0), \quad r\in(0,a),\ \ \theta\in(0,2\pi),\ \ z=\ell, \tag{B.6b}$$

$$\frac{\partial}{\partial n}G(\mathbf{r},\mathbf{r}_0) = 0, \quad r=0,\ \ \theta\in(0,2\pi),\ \ z\in(0,\ell). \tag{B.6c}$$

The solution for p is given by

$$p(\mathbf{r}) = \frac{\mathrm{j}k_0\rho_0c_0}{1-K_v}\left[\iint_{S_t} v_t(\mathbf{r}_0)G(\mathbf{r},\mathbf{r}_0)\,\mathrm{d}S_0 + \iint_{S_r} v_R(\mathbf{r}_0)G(\mathbf{r},\mathbf{r}_0)\,\mathrm{d}S_0\right] - \mathrm{j}k_0\rho_0c_0\iint_{\sigma_c} y_c(\mathbf{r}_0)p(\mathbf{r}_0)G(\mathbf{r},\mathbf{r}_0)\,\mathrm{d}S_0, \tag{B.7}$$

where S_t and S_r are, respectively, the surfaces of the transmitter and receiver diaphragms, and $y_c = Y_c/\sigma_c$, Green's function being taken as [9]

$$G(\mathbf{r},\mathbf{r}_0) = \sum_{\mu,v=0,1\ldots,d=c,s} g_{\mu v}(z,z_0)\psi^d_{\mu v}(r_0,\theta_0)\psi^d_{\mu v}(r,\theta), \tag{B.8}$$

where the eigenfunctions $\psi^d_{\mu v}$, the superscript d standing for either $\sin\mu\theta$ or $\cos\mu\theta$, satisfy Neumann boundary conditions, Eq. (B.7) leads readily to the acoustic pressure

$$p(r,\theta,z) = \sum_{\mu,v,d} p^d_{\mu v}(z)\psi^d_{\mu v}(r,\theta) \tag{B.9a}$$

with

$$p^d_{\mu v}(z) = \frac{\mathrm{j}k_0\rho_0c_0}{1-K_v}[g_{\mu v}(z,0)\langle v_t|\psi^d_{\mu v}\rangle_t + g_{\mu v}(z,\ell)\langle v_R|\psi^d_{\mu v}\rangle_r] - \mathrm{j}k_0\rho_0c_0g_{\mu v}(z,\ell_c)\sum_{\mu',v',d'} p^{d'}_{\mu' v'}(\ell_c)\langle y_c\psi^{d'}_{\mu' v'}|\psi^d_{\mu v}\rangle_{\sigma_c}, \tag{B.9b}$$

where $\langle v_t|\psi^d_{\mu v}\rangle_t$ is the integral over the surface S_t of $v_t(r,\theta)\psi^d_{\mu v}(r,\theta)$ and $\langle v_R|\psi^d_{\mu v}\rangle_r$ is the integral over the surface S_r of $v_R(r,\theta)\psi^d_{\mu v}(r,\theta)$, and where

$$\psi^c_{\mu v}(r,\theta) = \frac{1}{a_\mu b_{\mu v}}\cos\mu\theta J_\mu(k_{w\mu v}r), \tag{B.10a}$$

$$\psi^s_{\mu v}(r,\theta) = \frac{1}{a_\mu b_{\mu v}}\sin\mu\theta J_\mu(k_{w\mu v}r), \tag{B.10b}$$

where $1/(a_\mu b_{\mu v})$ is the normalization coefficient, the functions J_μ the cylindrical Bessel functions of the first kind, and $k_{w\mu v}$ the corresponding eigenvalues such as

$$k_{w\mu v}a = \gamma_{\mu v}, \tag{B.11}$$

where $\gamma_{\mu v}$ is the $(v+1)$th zero of the first derivative with respect to r of the Bessel function $J_\mu(k_{w\mu v}r)$.

As long as the accurate velocity of the diaphragms remains unknown, it is not possible to derive from expression (B.9a) of the sound pressure a sufficiently accurate expression of the acoustic transfer admittance Y_T, that is the quantity of interest here. Indeed, some approximations can be suggested, as in Ref. [9], to express the admittance Y_T, but they lead to some uncertainties. A more advanced modelling which would account for the velocity profiles of the diaphragms of the microphones in the formulation, that is to say in the modelling of the microphones themselves, would provide more accurate expressions for both the acoustic transfer admittance Y_T and the electrical transfer admittance Y_E, reducing these uncertainties.

Appendix C. Integration constants of Eqs. (13a, b)

The integration constants A, B, C, and D of Eqs. (13a, b) are given by

$$A = \frac{Sv_t}{Y_i(1-B) + Y_b(1+B)}, \tag{C.1a}$$

$$B = -\mathrm{e}^{-2\mathrm{j}k_z\ell_c}\frac{Y_c + D\mathrm{e}^{2\mathrm{j}k_z\ell_c}(Y_c - 2Y_i)}{(Y_c + 2Y_i) + D\mathrm{e}^{2\mathrm{j}k_z\ell_c}Y_c}, \tag{C.1b}$$

$$C = A\frac{\mathrm{e}^{-\mathrm{j}k_z\ell_c} + B\mathrm{e}^{\mathrm{j}k_z\ell_c}}{\mathrm{e}^{-\mathrm{j}k_z\ell_c} + D\mathrm{e}^{\mathrm{j}k_z\ell_c}}, \tag{C.1c}$$

$$D = \mathrm{e}^{-2\mathrm{j}k_z\ell}\frac{Y_i - (Y_r + Y_b)}{Y_i + (Y_r + Y_b)}. \tag{C.1d}$$

Appendix D. Input impedance of a slit open on free space

The slit considered, sketched in Fig. 2, is set around the lateral surface of the coupler at $r = a$ and $z = \ell_c$ (see Fig. 1). The thickness e of the slit is much smaller than the length ℓ of the coupler. Its outer radius is denoted R, and its output acoustic load is assumed to be described by the Dirichlet condition (free-field condition).

The acoustic field inside the slit is governed by the propagation equations for harmonic motion (Eqs. (A.21) and (A.22)):

$$\left[\frac{\partial^2}{\partial r^2} + \frac{1}{r}\frac{\partial}{\partial r} + \chi^2\right]p(r) = 0, \tag{D.1}$$

where

$$\chi^2 = k_0^2\frac{1 + (\gamma-1)K_h^s}{1 - K_v^s}, \quad \mathrm{Re}(\chi) > 0 \text{ and } \mathrm{Im}(\chi) < 0 \tag{D.2}$$

and (Eq. (A.23))

$$K_{v,h}^s = \frac{\tan(k_{v,h}e/2)}{k_{v,h}e/2}. \tag{D.3}$$

The solution of Eq. (D.1), subjected to the boundary condition $p(r = R) = 0$, is given by

$$p(r) = A_s[J_0(\chi r) + B_s Y_0(\chi r)] \tag{D.4}$$

with

$$B_s = -\frac{J_0(\chi R)}{Y_0(\chi R)}. \tag{D.5}$$

Applying the r-component of Eq. (A.9) to express the particle velocity $v_r(a)$ at the input of the slit, the acoustic input admittance Y_c^s at $r = a$ takes the form

$$Y_c^s = \frac{2\pi ae\langle v_r(a)\rangle_{z_s}}{p(a)} = \frac{aY'}{R}\frac{J_1(\chi a) + B_s Y_1(\chi a)}{J_0(\chi a) + B_s Y_0(\chi a)}, \tag{D.6}$$

where $\langle v_r(a)\rangle_{z_s}$ is the mean value across the thickness of the slit of the velocity $v_r(a)$, and where the admittance Y' is given by

$$Y' = \frac{2\pi Re}{\mathrm{j}\rho_0 c_0}\sqrt{[1 + (\gamma-1)K_h^s][1 - K_v^s]}. \tag{D.7}$$

It is worth noting that an accurate approximate expression can be substituted to expression (D.6) of the admittance Y_c^s both in the lower frequency range (in the limit of a small value of $|k_{v,h}e|$, Eqs. (D.2), (D.3),

(A.5b), and (A.6b)) and in the higher frequency range (asymptotic behaviour for large values $|k_{h,v}e|$, Eqs. (D.2), (D.3), (A.5b), and (A.6b)), the usual thickness "e" of this component being given (as opposed to the coupler of the reciprocity calibration device for which the only asymptotic behaviour is an accurate approximation, irrespective of the frequency as mentioned at the end of Section 3, Eq. (20)). But, in the intermediate frequency range, namely here roughly from 100 Hz to 10 kHz, expression (D.6) of Y_c^s must be used without approximation because, in this frequency range, expressions (A.5b) and (A.6b) of k_v and k_h, respectively, which appear in Eqs. (D.2) and (D.3) of the complex wavenumber χ, yield (for $e = 71.2\,\mu\text{m}$)

$$1 < |k_{v,h}e| < 10.$$

In the lower frequency range (up to roughly 100 Hz) the approximate expression of Y_c^s (Eq. (D.6)) is given by

$$Y_c^s \approx \frac{2\pi e^3}{12\mu \ln(R/a)} \tag{D.8}$$

showing a purely resistive behaviour. Note that at 100 Hz (for $e = 71.2\,\mu\text{m}$, $a = 4.65\,\text{mm}$ and $R = 8.5\,\text{mm}$),

$$Y_c^s \approx 1.73 \times 10^{-8}\,\text{m}^3\,\text{s}^{-1}\,\text{Pa}^{-1}.$$

Appendix E. Input impedance of a set of four cylindrical tubes

The four similar cylindrical tubes considered are set around the lateral surface of the coupler at $r = a$, $z = \ell_c$ and $\theta = 0$, $\pi/2$, π, $3\pi/2$. Their radius a_T is much smaller than the length ℓ of the coupler. Their axes are denoted x_t, the origin $x_t = 0$ being chosen at the input of the tube, and their length is denoted ℓ_T.

The acoustic field inside each tube is governed by the propagation Eq. (A.17), written as follows:

$$\left[\frac{\partial^2}{\partial x_t^2} + k_t^2\right] p(x_t) = 0,$$

where the wavenumber k_t is given by the right-hand side of Eq. (A.20).

The solution is given by

$$p(x_t) = A_t(\mathrm{e}^{-\mathrm{j}k_t x_t} + B_t \mathrm{e}^{\mathrm{j}k_t x_t}), \tag{E.1}$$

where the integration constant B_t is given by the boundary condition at $x_t = \ell_T$ which is either a Dirichlet condition (output free field) or a mixed condition (output load impedance Z_L).

Applying the x_t-component of Eq. (A.9) to express the mean value (across the section of the tube) of the particle velocity $v(x_t = 0)$ at the input of each tube, the input acoustic admittance Y_c^t of each tube, the ratio of the volume velocity to the acoustic pressure at $x_t = 0$, is given by

$$Y_c^t = \frac{\pi a_T^2 v(x_t = 0)}{p(x_t = 0)} = Y_i \frac{1 + Z_L Y_i \tanh(\mathrm{j}k_t \ell_T)}{\tanh(\mathrm{j}k_t \ell_T) + Z_L Y_i} \tag{E.2}$$

the iterative admittance Y_i being given by Eq. (17a) replacing the radius a by a_T.

If the tubes are open on a free space at $x_t = \ell_T$, the loading impedance Z_L disappears and the admittance Y_c^t reduces to

$$Y_c^t = \frac{Y_i}{\tanh(\mathrm{j}k_t \ell_T)}. \tag{E.3}$$

It is worth noting that accurate approximate expression can be substituted into expression (E.2) or (E.3) of the admittance Y_c^t both in the lower frequency range (in the limit of a small value of $|k_{v,h}a_T|$, Eqs. (A.18), (A.19), (A.5b), and (A.6b)) and in the higher frequency range (asymptotic behaviour for large values of $|k_{v,h}a_T|$, Eqs. (A.18), (A.19), (A.5b), and (A.6b)), the usual radius "a_T" of such components being given (as opposed to the coupler of the reciprocity calibration device for which the only asymptotic behaviour is an accurate approximation, irrespective of the frequency, as mentioned at the end of Section 3, Eq. (20)). But, in the intermediate frequency range, namely here roughly from 100 Hz to 10 kHz, expression (E.3) of Y_c^t must be used without approximation because, in this frequency range, expressions (A.5b) and (A.6b) of k_v and k_h,

respectively, which appear in Eqs. (A.18) and (A.19) of the complex wavenumber k_t, yield (for $a_T = 225\,\mu\text{m}$)

$$1 < |k_{v,h} a_T| < 10.$$

In the lower frequency range (up to roughly 100 Hz) the approximate expression of Y_c^t (Eq. (E.3)) is given by

$$Y_c^t \approx \frac{\pi a_T^4}{8\mu \ell_T} \tag{E.4}$$

showing a purely resistive behaviour. Note that at 100 Hz (for $a_T = 225\,\mu\text{m}$ and $\ell_T = 3.8\,\text{mm}$),

$$Y_c^t \approx 1.29 \times 10^{-8}\,\text{m}^3\,\text{s}^{-1}\,\text{Pa}^{-1}.$$

In the following, the impedance Z_L is calculated when the outputs of the tubes are loaded by a closed small annular cavity as sketched in Fig. 3 (this kind of shape is used in artificial ears [12]).

The annular cavity comprises two annular slits (labelled below $i = 1, 2$) having the same behaviour as the annular slit modelled in the previous appendix (D).

Therefore, the solution for the pressure variation in each cavity is given by (Eq. (D.4)):

$$p_i(r) = A_i[J_0(\chi_i r) + B_i Y_0(\chi_i r)] \tag{E.5}$$

with $i = 1$ for the first slit (thickness e_1, inner and outer radius, respectively, R_1 and R_2) and $i = 2$ for the second slit (thickness e_2, inner and outer radius, respectively, R_2 and R_3), with $R_1 = a + \ell_T$, and where (Eq. (A.22))

$$\chi_i^2 = k_0^2 \frac{1 + (\gamma - 1)K_h^i}{1 - K_v^i}, \quad \text{Re}(\chi_i) > 0 \text{ and } \text{Im}(\chi_i) < 0 \tag{E.6}$$

with

$$K_{v,h}^i = \frac{\tan(k_{v,h} e_i/2)}{k_{v,h} e_i/2}. \tag{E.7}$$

The integration constants B_i are given by the continuity of the volume velocities and pressures at $r = R_2$ and by the boundary condition at $r = R_3$ (thermal boundary layer admittance, Eq. (8b)). Then, applying the r-component of Eq. (A.9) to express the mean value (across the section of the slit) of the particle velocity $v_r(R_1)$, the acoustic input impedance Z_L at the output of each tube is written as

$$Z_L = \frac{4p_1(R_1)}{2\pi R_1 e_1 v_{r1}(R_1)} = \frac{4R_3}{R_1 Y_1'} \frac{J_0(\chi_1 R_1) + B_1 Y_0(\chi_1 R_1)}{J_1(\chi_1 R_1) + B_1 Y_1(\chi_1 R_1)}, \tag{E.8}$$

where

$$B_1 = -\frac{Y_1' J_1(\chi_1 R_2)[J_0(\chi_2 R_2) + B_2 Y_0(\chi_2 R_2)] - Y_2' J_0(\chi_1 R_2)[J_1(\chi_2 R_2) + B_2 Y_1(\chi_2 R_2)]}{Y_1' Y_1(\chi_1 R_2)[J_0(\chi_2 R_2) + B_2 Y_0(\chi_2 R_2)] - Y_2' Y_0(\chi_1 R_2)[J_1(\chi_2 R_2) + B_2 Y_1(\chi_2 R_2)]}, \tag{E.9}$$

$$B_2 = -\frac{J_0(\chi_2 R_3) - (Y_2'/Y_b') J_1(\chi_2 R_3)}{Y_0(\chi_2 R_3) - (Y_2'/Y_b') Y_1(\chi_2 R_3)} \tag{E.10}$$

with

$$Y_i' = \frac{2\pi R_{i+1} e_i}{\text{j}\rho_0 c_0} \sqrt{[1 + (\gamma - 1)K_h^i][1 - K_v^i]}, \tag{E.11}$$

for $i = 1$ or 2, and

$$Y_b' = \frac{2\pi R_3 e_2}{\rho_0 c_0} \frac{1 + \text{j}}{\sqrt{2}} \sqrt{k_0}(\gamma - 1)\sqrt{\ell_h}. \tag{E.12}$$

References

[1] M.R. Moldover, J.B. Mehl, M. Greenspan, Gas-filled spherical resonators: theory and experiment, *Journal of the Acoustical Society of America* 79 (1986) 253–272.
[2] P.M. Morse, K.U. Ingard, *Theoretical Acoustics*, McGraw-Hill, New York, 1968.
[3] M. Bruneau, T. Scelo (translator and contributor), *Fundamentals of Acoustics*, ISTE, UK, USA, 2006.
[4] J.-P. Dalmont, Acoustic impedance measurement, part 1: a review, *Journal of Sound and Vibration* 243 (2001) 427–439.
[5] J.-P. Dalmont, Acoustic impedance measurement, part 2: a new calibration method, *Journal of Sound and Vibration* 243 (2001) 441–459.
[6] S. Ballantine, Technique of microphone calibration, *Journal of the Acoustical Society of America* 3 (1932) 319–360.
[7] International Electrotechnical Commission IEC 61094-2, Measurement microphones, part 2: Primary method for pressure calibration of laboratory standard microphones by the reciprocity technique, 1992.
[8] C. Guianvarc'h, J.-N. Durocher, M. Bruneau, A.-M. Bruneau, Acoustic transfer admittance of cylindrical cavities, *Journal of Sound and Vibration* 292 (2006) 595–603.
[9] C. Guianvarc'h, J.-N. Durocher, M. Bruneau, A.-M. Bruneau, Improved formulation of the acoustic transfer admittance of cylindrical cavities, *Acta Acustica united with Acustica* 92 (2006) 345–354.
[10] M. Bruneau, Machines thermiques, capteur gyrométrique et métrologie acoustique en application des propriétés des couches limites thermo-visqueuses, Proceeding, 8ème Congrès Français d'Acoustique (invited paper, Tours (France)), 2006.
[11] K.O. Ballagh, Acoustical admittance of cylindrical cavities, *Journal of Sound and Vibration* 112 (1987) 567–569.
[12] International Electrotechnical Commission IEC 60318-1, Electroacoustics—Simulators of human head and ear—part 1: Ear simulator for the calibration of supra-aural earphones, 1998.